## Cavity-Enhanced Two-Photon Interference using Remote Quantum Dot Sources

V. Giesz, <sup>1</sup> S. L. Portalupi, <sup>1,2</sup> T. Grange, <sup>3,4</sup> C. Antón, <sup>1,5</sup> L. De Santis, <sup>1</sup> J. Demory, <sup>1</sup> N. Somaschi, <sup>1</sup> I. Sagnes, <sup>1</sup> A. Lemaître, <sup>1</sup> L. Lanco, <sup>1,6</sup> A. Auffeves, <sup>3,4</sup> and P. Senellart <sup>1,7</sup>, \*

<sup>1</sup>Laboratoire de Photonique et de Nanostructures, CNRS,

UPR20, Route de Nozay, 91460 Marcoussis, France

<sup>2</sup>Institut für Halbleiteroptik und Funktionelle Grenzflächen, Universität Stuttgart, 70569 Stuttgart, Germany

<sup>3</sup>Université Grenoble Alpes, 38000 Grenoble, France

<sup>4</sup> CNRS, Institut Néel, "Nanophysique et semiconducteurs" group, 38000 Grenoble, France

<sup>5</sup>Departamento de Física de Materiales, Universidad Autónoma de Madrid, Madrid 28049, Spain

<sup>6</sup> Université Paris Diderot - Paris 7, 75205 Paris CEDEX 13, France

<sup>7</sup> Physics Department, Ecole Polytechnique, F-91128 Palaiseau Cedex, France

(Dated: December 3, 2024)

The generation of indistinguishable photons from a solid-state emitter like a semiconductor quantum dot is often limited by dephasing processes. It is known that accelerating the spontaneous emission of the quantum dot can greatly improve the indistinguishability of successively emitted photons. Here we show that cavity quantum electrodynamics can also efficiently improve the quantum interference between remote quantum dot sources. The quantum interference of photons emitted by two separate quantum dot-cavity devices is investigated both experimentally and theoretically. Controlling the spontaneous emission on one source is shown to efficiently overcome the detrimental effect of pure dephasing on the other one. Our experimental observations and calculations demonstrate that cavity quantum electrodynamics is a powerful tool for the scalability of a quantum dot-based quantum network.

PACS numbers: 78.67.Hc, 42.50.Ar, 42.50.Dv, 42.50.Pq, 42.50.St

Recent years have seen impressive progresses in the implementation of quantum functionalities using semiconductor quantum dots (QDs). The strong anharmonicity of the QD energy levels [1] has been used to generate flying quantum bits in the form of single-photons [2] or entangled photon pairs [3, 4], to map and optically manipulate the quantum information encoded onto a single stationary electron [5, 6] or hole spin [7] as well as to implement optical logic gates [8–10]. The potential of QD-based single-photon sources lies in their deterministic and pure quantum statistics, as opposed to the parametric down-conversion sources currently used in quantum optics. At saturation, the QD emits a single-photon with a probability close to one, with an evanescent probability of emitting a second photon. To fully benefit from this statistic, novel strategies have been developed to efficiently collect emitted photons from the high refractive index materials such as inserting the QD in a nanowire on a metallic mirror [11] or in a micropillar cavity [12].

Since the first demonstration in 2002 [13], the coalescence of photons successively emitted by a single QD has been widely investigated. Various strategies have been developed to minimize the environment-induced dephasing (phonons, charge noise). One approach consists in using a strictly resonant excitation to create directly the carriers into the QD state and reduce the time-jitter of the photon emission [9, 14–17]. Another approach consists in using the Purcell effect by inserting the QD in a microcavity. The acceleration of spontaneous emission reduces the effect of dephasing [12, 13, 18] and leads to an efficient extraction of photons: ultra-bright sources of

highly indistinguishable photons were recently reported using this approach [12].

The scalability of a quantum network based on QDs relies on the possibility of interconnecting two QD devices. Pioneer steps have been made in this direction making use of the two-photon interference between singlephotons emitted by remote QDs in planar structures [19–22]. Under non-resonant excitation, the coalescence probability is limited by the dephasing processes on each source [19–21]. The use of a resonant, narrow excitation line has led to a higher coalescence probability [22] by inducing an effective filtering of the events where the transitions of both QDs are at the laser frequency. This technique allows getting around spectral diffusion, vet at the expense of the source brightness. In the present work, we demonstrate that the Purcell effect, which allows efficient collection of photons, is also a powerful tool to improve the coalescence probability from remote sources. We study for the first time the quantum interference of remote QD sources, each of them consisting of a single InGaAs QD embedded in a microcavity. Accelerating the spontaneous emission of one source is shown to efficiently reduce the effect of pure dephasing of the other one.

The QD-micropillar devices are fabricated from the same planar microcavity sample consisting of a bottom (top) Bragg mirror with 32 (18)  $\lambda/4$  GaAs/Al<sub>0.95</sub>Ga<sub>0.05</sub>As layers, surrounding an adiabatic cavity embedding a dilute InGaAs QD layer in its center (see Ref.[23, 24] for details). Micropillar cavities are laterally centered on single selected QDs with a 50 nm accuracy using the optical *in-situ* lithography technique

[25]. Two *in-situ* lithography steps were performed on two parts of the same 1 cm<sup>2</sup>-area sample. After the pillar etching, the sample was cleaved in two pieces, which were inserted in two separated cryostats with independent temperature-tuning [see Fig. 1(a)]. Two pillars presenting the same diameter in each cryostat are studied, named hereafter QD A and QD B.

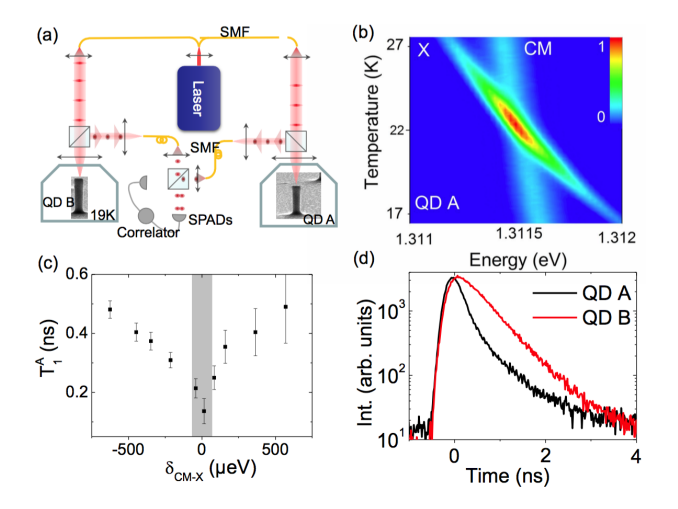


FIG. 1: (a) Scheme of experimental setup (see text for details). (b) QD A emission as function of temperature and energy. The QD A exciton line (X) is resonant to the bare cavity mode (CM) at 22 K. (c) Decay time of QD A exciton line  $(T_1^A)$  deconvoluted from the temporal resolution of the setup vs.  $\delta_{\rm CM-X}$ . The spectral range used for the two-source interference is marked with a grey, vertical stripe. (d) Decay of QD A (QD B) emission line in a black (red) color line for  $\delta_{\rm CM-X}=0$ .

For both devices, the QD resonance is spectrally very close to the mode resonance at 10 K. The fine spectral matching is obtained by increasing temperatures that shift the exciton lines to lower energies throughout the CM resonance [Fig.1(b)]. Figure 1(c) shows the decay time of the QD A exciton line as a function of the energy detuning  $\delta_{\text{CM-X}} = E_{CM} - E_X$ . When reducing  $\delta_{\text{CM-X}}$ , the X decay time decreases, to reach a minimum value of  $T_1^A = 140 \pm 40$  ps at resonance ( $\delta_{\text{CM-X}} = 0$ ). As recently shown, coupling to acoustic phonons results in an effective Purcell factor that is smaller than the one obtained considering a two-level system only coupled to the CM [23]. For QD A, the decay time  $T_1^A$  at resonance corresponds to an effective Purcell factor around  $10 \pm 2$ , considering a radiative lifetime of 1.3 ns for the same QDs in bulk. A similar study performed on QD B gives a lifetime of  $T_1^B = 470 \pm 30$  ps at resonance. Although QD B is also spatially located at the center of the pillar, a smaller effective Purcell factor is measured showing a stronger coupling to phonons. The setup used for QD A could be carefully calibrated to measure the source brightness: at resonance a brightness of  $74 \pm 5\%$ 

is collected in the microscope objective with a 0.4 numerical aperture. The experimental configuration on the other setup did not allow such a calibration for QD B.

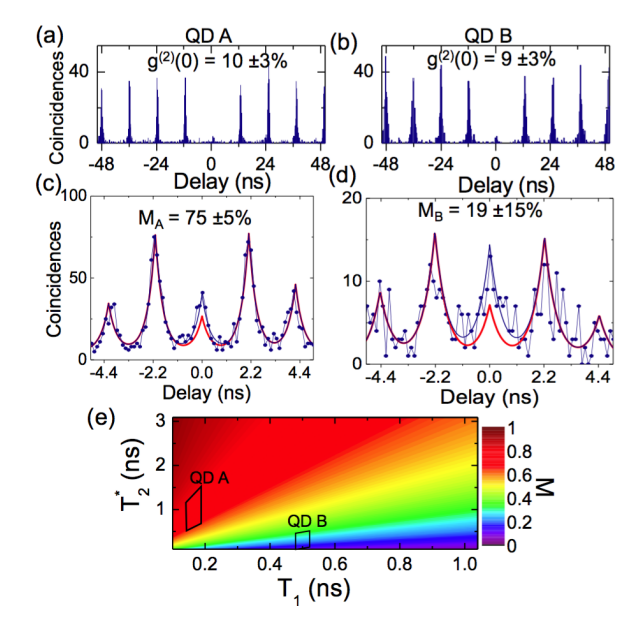


FIG. 2: Measured autocorrelation function of QD A (a) and QD B (b) exciton lines. (c,d) Correlation histograms measuring the indistinguishability of photons successively emitted by QD A and QD B, respectively. Black lines are a fittings to the experimental data with  $M_A = 75\%$  for QD A and  $M_B = 19\%$ . As a comparison, the red lines are the calculated curves for M = 1, considering the measured values for  $g^{(2)}(0)$ ,  $\epsilon$ , R and T values. (e) Calculated M as a function of  $T_1$  and  $T_2^*$ . The areas corresponding to QD A and QD B are indicated.

A single Ti-Sapphire laser, providing 3 ps-long light pulses at a 82 MHz repetition rate, is used to excite both devices, so as to obtain synchronized single-photons from each source. To obtain a good single-photon purity in a regime of strong Purcell effect, the QD devices are excited with a laser energy below the wetting layer resonance [26]. A common excitation state, at 1.370 eV, was found for both QDs. The single-photon emission is quantified by sending the photons emitted by each device, after coupling into a single mode fiber (SMF), to an a Hanbury Brown-Twiss setup: photons impinge on a 50:50 beam splitter (BS) with outputs coupled to spectrometers for spectral filtering and single-photon avalanche diodes (SPADs).

Figures 2(a,b) present the autocorrelation functions measured for both devices. A good single-photon purity is obtained for both with an integrated  $g^{(2)}(0)$  for the zero delay peaks of  $g_A^{(2)}(0) = 10 \pm 3\%$  for QD A and  $g_B^{(2)}(0) = 9 \pm 3\%$  for QD B. To measure the indistinguishability of successively emitted photons for each source, each device is excited twice using an additional 2.3 ns delay line on the excitation laser line [Figs. 2(c,d)]. The emitted single-photons, coupled into the SMF, are non-

deterministically split using a 50:50 fiber-based BS and then sent to the two inputs of a cube BS. A 2.3 ns fiber delay line is added on one of the outputs of the fiber BS so that the two photons reach the BS at the same time. A polarizer is inserted between the collection objective and the SMF to collect photons polarized along the QD axes. This polarization is further adjusted before the two inputs of the BSs with polarizers and fiber-paddles. The temporal coincidences are measured with two SPADs at the outputs of the cube BS after spectral filtering with spectrometers (17 pm resolution). The photon indistinguishability is measured through the mean wave packet overlap (M) as defined in Ref. [13]. For perfectly indistinguishable photons  $M=1, g^{(2)}(0)=0$  and perfect experimental setup, no signal should be observed at zero delay. For the present experimental configuration, the measured area of the peak at zero delay  $(A_0)$  compared to the area of the lateral peaks at  $\pm$  2.3 ns  $(A_{\pm 2.3 \text{ns}})$ allows deducing M using:

$$M = \frac{1}{(1-\epsilon)^2} \left[ 2g^{(2)}(0) + \frac{R^2 + T^2}{2RT} - \frac{A_0}{A_{-2.3\text{ns}} + A_{+2.3\text{ns}}} \left( 2 + g^{(2)}(0) \frac{(R^2 + T^2)}{RT} \right) \right]$$
(1)

where  $\epsilon=0.88\pm0.03$  is the interference fringe contrast measured with a coherent laser, and  $R=0.40\pm0.02$  and  $T=0.50\pm0.02$  are the BS intensity reflection and transmission, respectively. From these measurements, we deduce M for each source: it is as high as  $M_A=75\pm5\%$  for QD A, but only  $M_B=19\pm15\%$  for QD B. Note that using a single laser to excite both QDs did not allow optimizing simultaneously  $M_A$  and  $M_B$ . The excitation wavelength was chosen to optimize  $M_A$ .

Recent works have shown that the indistinguishability of photons successively emitted by a QD depends on the excitation conditions and is mostly limited by charge noise around the QD [12, 21, 27]. The fluctuations of the electrostatic environment lead to a time dependent variation of the X energy (spectral diffusion) or pure dephasing mechanisms, depending on whether the time scale of the charge fluctuations is longer or shorter than the QD radiative lifetime [28]. In the present case, we have modeled the full set of data (including the two-source interference presented below), with both approaches and they can account equally well for our experimental observations. As a result, we choose a pure dephasing description, which allows deriving analytical equations for the two-source interference.

For photons emitted by a single source, the photon in distinguishability is given by  $M=\frac{T_2^*}{T_2^*+2T_1}=\frac{\gamma}{\gamma+\gamma^*},$  where  $T_1$   $(\gamma)$  is the decay time (rate) of the X transition and  $T_2^*$   $(\gamma^*/2)$  is the pure dephasing time (rate). We deduce a dephasing  $T_2^*$  between 500 ps and 1500 ps (50 ps and 450 ps) for QD A (QD B) considering  $T_1^A=140\pm40$ 

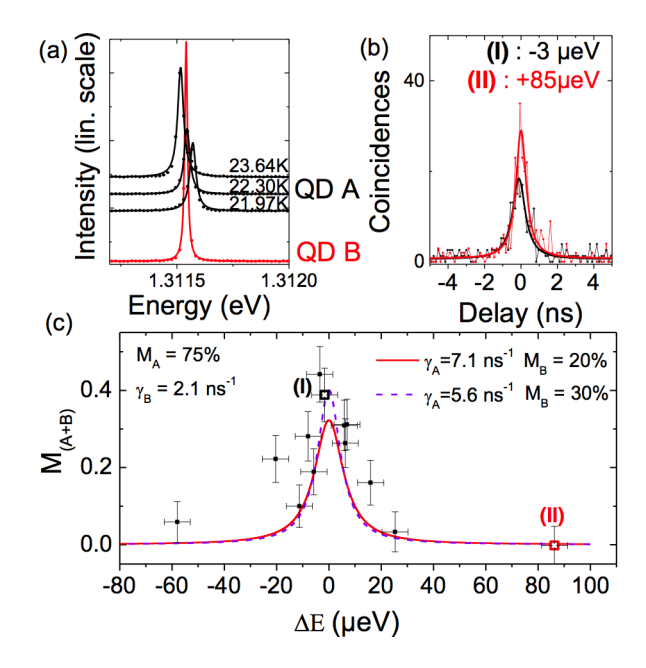


FIG. 3: (a) Emission spectra for QD B at 19 K (red bottom line) and QD A for various temperatures (black lines) . (b) Measured correlation of the two-source interference at two values of  $\Delta E$ : (I)  $-3~\mu \text{eV}$  (black) and (II)  $+85~\mu \text{eV}$  (red). Full lines are fits to the experimental data. (c) Measured  $M_{(A+B)}$  as a function of  $\Delta E$ . Lines are fits to the experimental data using the parameters indicated in the legend. The particular detunings (I) and (II) are labeled in the panel.

ps  $(T_1^B = 500\pm30 \text{ ps})$ . Figure 2(e) presents a color map of the photon indistinguishability M as a function of  $T_1$  and  $T_2^*$ , highlighting how reducing  $T_1$  through Purcell effect increases M for a given  $T_2^*$ . The regions of parameters allowing to account for our experimental observations are indicated for each device.

The two-source interference is performed for different spectral detunings of the QDs: while QD B is kept to a fixed temperature where  $\delta^B_{\mathrm{CM-X}} = 0$ , the temperature of QD A is varied over 1.7 K to tune the spectral detuning  $\Delta E = E^B_X - E^A_X$  of the two sources [Fig. 3(a)]. The QD excitations are respectively delayed so that the generated single-photons impinge simultaneously (with a temporal accuracy of  $\sim 8$  ps) on the two inputs of the BS. The photon correlation on the two output SPADs allows deducing the mean wave packet overlap using the area  $A_0$  of the zero delay peak and the area  $A_{12.2\mathrm{ns}}$  of the 12.2 ns peaks coming from the laser repetition rate:

$$M_{(A+B)} = \frac{1}{(1-\epsilon)^2} \left[ \frac{g^{(2)}_A(0) + g^{(2)}_B(0)}{2} + \frac{R^2 + T^2}{2RT} - \frac{(R+T)^2}{2RT} \frac{A_0}{A_{12.2\text{ns}}} \right]$$
(2)

Figure 3(b) presents the zero delay peak of the correlation curve for the sources detuning  $\Delta E = -3 \mu \text{eV}$  (black)

and +85  $\mu eV$  (red). A clear decrease of the zero delay peak area is observed when the two sources are in resonance, showing the increased photon coalescence probability. Figure 3(c) presents the measured  $M_{(A+B)}$  as a function of  $\Delta E$ . For large detunings, it is observed that  $M_{(A+B)}=0$ , as expected for distinguishable photons. At  $\Delta E=0$ , a mean wavepacket overlap  $M_{(A+B)}=40\pm4\%$  is observed. This value constitutes the current state-of-the-art for a two-source interference under non-resonant excitation [21]. Figure 3(c) also shows that the two-photon interference takes place on a spectrally broad spectral range, with a full width at half maximum of  $\sim 15\pm5~\mu eV$ .

If both sources undergo pure dephasing,  ${\cal M}_{(A+B)}$  for the two photons overlap is:

$$M_{(A+B)} = \frac{\gamma_A \gamma_B}{\gamma_A + \gamma_B} \frac{\gamma_A + \gamma_B + \gamma_A^* + \gamma_B^*}{(\frac{\Delta E}{\hbar})^2 + \frac{1}{4} (\gamma_A + \gamma_B + \gamma_A^* + \gamma_B^*)^2}$$
(3)

(see supplementary for details) As shown in Fig. 3(c), our experimental observations can well be reproduced with  $M_A$ =0.75,  $\gamma_B = 2.1 \text{ ns}^{-1}$ , 5.6 <  $\gamma_A < 7.1 \text{ ns}^{-1}$ and  $0.2 < M_B < 0.3$ , which are consistent with the measurements performed on each source within the error bars. The linewidth of the two photon interference is given by the sum of each emitter linewidth. The strong Purcell effect on QD A, contributing through  $\gamma_A$ , leads to a significant increase of the spectral range over which the two-source quantum interference takes place. Another striking feature of the Purcell assisted two-source interference is that the coalescence probability reaches  $40 \pm 4\%$ , even if photons successively emitted by the QD B source present an overlap of only  $M_B = 19 \pm 15\%$ . In the following, we analyse in details how the two source interference is enhanced by use of Purcell effect.

Figure 4(a) presents the calculated  $M_{(A+B)}$  for  $\Delta E =$ 0 as a function of the decay time of QD A for various values of  $M_B$ . The lifetime of QD B is fixed to  $T_1^B = 450$ ps and  $M_A = 75\%$ . The vertical, dashed line indicates the situation where the two sources present the same decay time. The coalescence probability is optimal for sources with identical lifetime only for  $M_A \approx M_B$ . When  $M_B < M_A$ , the maximum probability of coalescence is obtained for an optimal value of  $T_1^A (T_{1,opt}^A)$  that depends on  $M_B$ : the lower the indistinguishability of successively emitted photons by QD B source, the stronger the Purcell factor on QD A should be to overcome the pure dephasing on QD B. In other words, the faster the decoherent processes on  $X_B$  are, the faster QD A emission should be to compensate them. The grey area in Fig. 4(a) presents the conditions reached in the current measurements where this effect is demonstrated.

For the optimal value  $T_{1,opt}^A$ , the coalescence probability of the two-source interference significantly exceeds  $M_B$ . Figure 4(b) presents in the left, vertical axis the best achievable overlap  $M_{(A+B)}$  as a function of  $M_B$ 

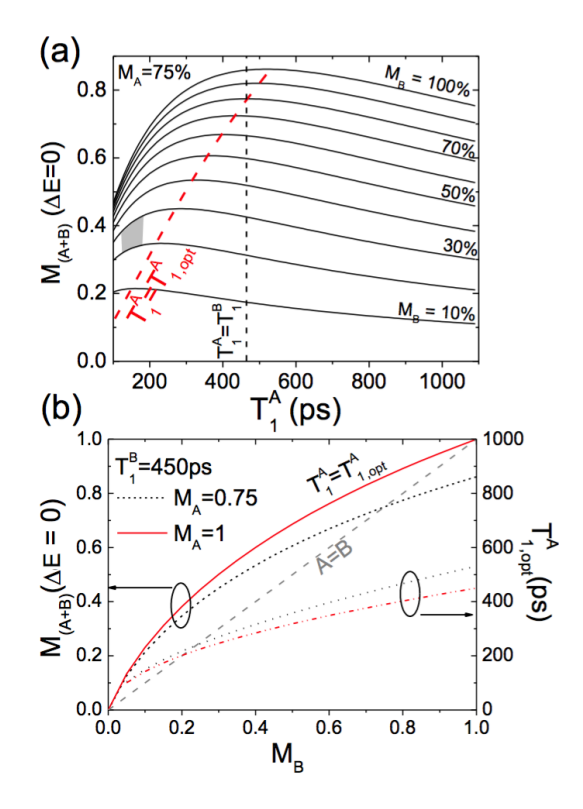


FIG. 4: (a) Calculated photon overlap  $M_{(A+B)}$  at  $\Delta E=0$  as a function of QD A decay time  $T_1^A$  (with a fixed  $M_A=75\%$ ) for different values of  $M_B$ . The decay time of QD B is fixed at  $T_1^B=470$  ps. Red, dashed line indicates the optimal values of  $T_{1,opt}^A$  where  $M_{(A+B)}(\Delta E=0)$  is maximum. The vertical, dashed line indicates the situation where the two sources present the same decay time. (b) (Left, vertical axis) Optimal photon overlap  $M_{(A+B)}(\Delta E=0)$  obtained at  $T_{1,A}=T_{1,opt}^A$  and  $T_1^B=470$  ps in a full, red (dashed, black) line for  $M_A=1$  ( $M_A=0.75$ ). The grey, dashed line indicates the indistinguishability when both sources are identical. (Right, vertical axis)  $T_{1,opt}^A$  decay time as function of  $M_B$  for a value of  $M_A=1$  (0.75) in a red, dot-dashed (black, dotted) line.

obtained with  $T_1^A = T_{1,opt}^A$  for the case of the present measurement  $M_A = 75\%$  (black, dotted line) and for  $M_A = 100\%$  (red, full line). The grey, dashed line allows comparing the best achievable overlap to the case where both sources are identical. The right, vertical axis shows the value of  $T_{1,opt}^A$  as function of  $M_B$  that renders the optimal coalescence probability  $M_{(A+B)}$ . For  $M_B < M_A$ , the best achievable overlap in the two-source experiment is significantly larger than the one obtained for photons successively emitted by QD B and exceeds the one obtained considering a source with the same lifetime.

In solid-state systems, where dephasing is a limitation to scalability, cavity quantum electrodynamics is shown, for the first time in a two-source experiment, to be a powerful asset. The Purcell effect, known to improve the indistinguishability of photons successively emitted by a single source, is shown to enhance the quantum interference of remote sources: accelerating the spontaneous emission on one device can reduce the effect of dephasing on another one. This result is crucial for the scalability of QD-based quantum networks, where the imperfections of one device can be efficiently compensated by a highly indistinguishable single-photon source with a controlled lifetime. Contrary to common intuition, our results demonstrate that the optimal photon coalescence is not always obtained for sources with identical temporal wavepackets.

This work was partially supported by the ERC starting grant 277885 QD-CQED, the French RENATECH network, the Labex NanoSaclay, the CHISTERA project SSQN and the EU FP7 grant 618072 (WASPS). C.A. acknowledges financial support from the Spanish FPU scholarship.

- \* Electronic address: pascale.senellart@lpn.cnrs.fr
- M. Bayer, O. Stern, P. Hawrylak, S. Fafard, and a. Forchel, Nature 405, 923 (2000).
- [2] P. Michler, a. Kiraz, C. Becher, W. V. Schoenfeld, P. M. Petroff, L. Zhang, E. Hu, and a. Imamoglu, Science 290, 2282 (2000).
- [3] N. Akopian, N. H. Lindner, E. Poem, Y. Berlatzky, J. Avron, D. Gershoni, B. D. Gerardot, and P. M. Petroff, Phys. Rev. Lett. 96, 130501 (2006).
- [4] R. M. Stevenson, R. J. Young, P. Atkinson, K. Cooper, D. a. Ritchie, and a. J. Shields, Nature 439, 179 (2006).
- [5] C. Emary, X. Xu, D. G. Steel, S. Saikin, and L. J. Sham, Phys. Rev. Lett. 98 (2007).
- [6] D. Press, T. D. Ladd, B. Zhang, and Y. Yamamoto, Nature 456, 218 (2008).
- [7] B. D. Gerardot, D. Brunner, P. a. Dalgarno, P. Ohberg, S. Seidl, M. Kroner, K. Karrai, N. G. Stoltz, P. M. Petroff, and R. J. Warburton, Nature 451, 441 (2008).
- [8] M. A. Pooley, D. J. P. Ellis, R. B. Patel, A. J. Bennett, K. H. A. Chan, I. Farrer, D. A. Ritchie, and A. J. Shields, App. Phys. Lett. 100, 211103 (2012).
- [9] Y.-M. He, Y. He, Y.-J. Wei, D. Wu, M. Atatüre, C. Schneider, S. Höfling, M. Kamp, C.-Y. Lu, and J.-W. Pan, Nat. Nanotechnol. 8, 213 (2013).
- [10] O. Gazzano, M. P. Almeida, a. K. Nowak, S. L. Portalupi, a. Lemaître, I. Sagnes, a. G. White, and P. Senellart, Phys. Rev. Lett. 110, 250501 (2013).
- [11] J. Claudon, J. Bleuse, N. S. Malik, M. Bazin, P. Jaffrennou, N. Gregersen, C. Sauvan, P. Lalanne, and J.-M. Gérard, Nat. Photonics 4, 174 (2010).
- [12] O. Gazzano, S. Michaelis de Vasconcellos, C. Arnold, a. Nowak, E. Galopin, I. Sagnes, L. Lanco, a. Lemaître, and P. Senellart, Nat. Commun. 4, 1425 (2013).
- [13] C. Santori, D. Fattal, J. Vucković, G. S. Solomon, and Y. Yamamoto, Nature 419, 594 (2002).
- [14] C. Matthiesen, A. N. Vamivakas, and M. Atatüre, Phys. Rev. Lett. 108, 093602 (2012).
- [15] R. Proux, M. Maragkou, E. Baudin, C. Voisin, P. Roussignol, and C. Diederichs, Phys. Rev. Lett. 114, 067401 (2015).
- [16] Y.-J. Wei, Y.-M. He, M.-C. Chen, Y.-N. Hu, Y. He,

- D. Wu, C. Schneider, M. Kamp, S. Höfling, C.-Y. Lu, and J.-W. Pan, Nano Letters 14, 6515 (2014).
- [17] M. Muller, S. Bounouar, K. D. Jons, M. Glassl, and P. Michler, Nat Phot. 8, 224 (2014).
- [18] S. Varoutsis, S. Laurent, P. Kramper, A. Lemaître, I. Sagnes, I. Robert-Philip, and I. Abram, Phys. Rev. B 72, 041303 (2005).
- [19] E. B. Flagg, A. Muller, S. V. Polyakov, A. Ling, A. Migdall, and G. S. Solomon, Phys. Rev. Lett. 104, 137401 (2010).
- [20] R. B. Patel, a. J. Bennett, I. Farrer, C. a. Nicoll, D. a. Ritchie, and a. J. Shields, Nat. Photonics 4, 632 (2009), arXiv:0911.3997.
- [21] P. Gold, a. Thoma, S. Maier, S. Reitzenstein, C. Schneider, S. Höfling, and M. Kamp, Phys. Rev. B 89, 035313 (2014).
- [22] W. B. Gao, P. Fallahi, E. Togan, a. Delteil, Y. S. Chin, J. Miguel-Sanchez, and a. Imamoğlu, Nat. Commun. 4, 2744 (2013).
- [23] S. L. Portalupi, G. Hornecker, V. Giesz, T. Grange, A. Lemaître, J. Demory, I. Sagnes, N. D. Lanzillotti-Kimura, L. Lanco, A. Auffèves, and P. Senellart, arXiv:1412.6146 [cond-mat.mes-hall] (2015).
- [24] M. Lermer, N. Gregersen, F. Dunzer, S. Reitzenstein, S. Höfling, J. Mørk, L. Worschech, M. Kamp, and A. Forchel, Phys. Rev. Lett. 108, 057402 (2012).
- [25] A. Dousse, L. Lanco, J. Suffczyński, E. Semenova, A. Miard, A. Lemaître, I. Sagnes, C. Roblin, J. Bloch, and P. Senellart, Phys. Rev. Lett. 101, 267404 (2008).
- [26] V. Giesz, O. Gazzano, A. K. Nowak, S. L. Portalupi, A. Lemaître, I. Sagnes, L. Lanco, and P. Senellart, Appl. Phys. Lett. 103, 033113 (2013).
- [27] A. V. Kuhlmann, J. Houel, A. Ludwig, L. Greuter, D. Reuter, A. D. Wieck, M. Poggio, and R. J. Warburton, Nat. Phys. 9, 570 (2013).
- [28] A. Berthelot, I. Favero, G. Cassabois, C. Voisin, C. Delalande, P. Roussignol, R. Ferreira, and J. M. Gerard, Nat Phys 2, 759 (2006).

## Supplemental Materials: Cavity-Enhanced Two-Photon Interference using Remote Quantum Dot Sources

V. Giesz, <sup>1</sup> S. L. Portalupi, <sup>1,2</sup> T. Grange, <sup>3,4</sup> C. Antón, <sup>1,5</sup> L. De Santis, <sup>1</sup> J. Demory, <sup>1</sup> N. Somaschi, <sup>1</sup> I. Sagnes, <sup>1</sup> A. Lemaître, <sup>1</sup> L. Lanco, <sup>1,6</sup> A. Auffeves, <sup>3,4</sup> and P. Senellart <sup>1,7,\*</sup>

<sup>1</sup>Laboratoire de Photonique et de Nanostructures, CNRS, UPR20, Route de Nozay, 91460 Marcoussis, France <sup>2</sup>Institut für Halbleiteroptik und Funktionelle Grenzflächen, Universität Stuttgart, 70569 Stuttgart, Germany <sup>3</sup>Université Grenoble Alpes, 38000 Grenoble, France

<sup>4</sup> CNRS, Institut Néel, "Nanophysique et semiconducteurs" group, 38000 Grenoble, France <sup>5</sup> Departamento de Física de Materiales, Universidad Autónoma de Madrid, Madrid 28049, Spain <sup>6</sup> Université Paris Diderot - Paris 7, 75205 Paris CEDEX 13, France <sup>7</sup> Physics Department, Ecole Polytechnique, F-91128 Palaiseau Cedex, France

## TWO-PHOTON WAVE PACKET OVERLAP

We consider two photon wave packets sent on the two input ports (denoted A,B) of a beam splitter. The normalized probability  $p_c$  of coincidence detection in the two output ports (denoted C,D) reads [S1]

$$p_c = \frac{\int dt_1 \int dt_2 g_{CD}^{(2)}(t_1, t_2)}{\left[\int dt \langle \hat{a}_C^{\dagger}(t) \hat{a}_C(t) \rangle\right] \left[\int dt \langle \hat{a}_D^{\dagger}(t) \hat{a}_D(t) \rangle\right]},$$
(S1)

with

$$g_{CD}^{(2)}(t_1, t_2) = \langle \hat{a}_C^{\dagger}(t_1) \hat{a}_D^{\dagger}(t_2) \hat{a}_D(t_2) \hat{a}_C(t_1) \rangle. \tag{S2}$$

The beam splitter generates a unitary transformation of the form

$$\begin{pmatrix} \hat{a}_C \\ \hat{a}_D \end{pmatrix} = \begin{pmatrix} \sqrt{T} & -\sqrt{R}e^{-i\phi} \\ \sqrt{R}e^{i\phi} & \sqrt{T} \end{pmatrix} \begin{pmatrix} \hat{a}_A \\ \hat{a}_B \end{pmatrix}.$$
(S3)

In the limit of single photon wavepackets (i.e.  $g_{AA}^{(2)} = 0$  and  $g_{BB}^{(2)} = 0$ ), and assuming no phase correlations between the two sources, it can be expressed in terms of the input fields A and B as:

$$g_{CD}^{(2)}(t,t+\tau) = T^2 \langle a_A^{\dagger}(t)a_A(t)\rangle \langle a_B^{\dagger}(t+\tau)a_B(t+\tau)\rangle + R^2 \langle a_A^{\dagger}(t+\tau)a_A(t+\tau)\rangle \langle a_B^{\dagger}(t)a_B(t)\rangle - TR \langle a_A^{\dagger}(t)a_A(t+\tau)\rangle \langle a_B^{\dagger}(t+\tau)a_B(t)\rangle - TR \langle a_A^{\dagger}(t+\tau)a_A(t)\rangle \langle a_B^{\dagger}(t)a_B(t+\tau)\rangle.$$
(S4)

Within the Markov approximation, the wave packets sent by the two-level systems in A and B initially excited at t = 0 reads:

$$\langle a_A^{\dagger}(t)a_A(t+\tau)\rangle = n_A \gamma_A e^{-\gamma_A t} e^{-i\omega_A \tau} e^{-(\gamma_A + \gamma_A^*)\tau/2}, \tag{S5}$$

$$\langle a_B^{\dagger}(t)a_B(t+\tau)\rangle = n_B \gamma_B e^{-\gamma_B t} e^{-i\omega_B \tau} e^{-(\gamma_B + \gamma_B^*)\tau/2}, \tag{S6}$$

where  $\gamma_A$  ( $\gamma_B$ ) is the radiative decay rate of the emitter A (resp. B),  $\omega_A$  ( $\omega_B$ ) is its angular frequency,  $\gamma_A^*/2$  ( $\gamma_B^*/2$ ) is its pure dephasing rate, and  $n_A$  ( $n_B$ ) is the probability of photon emission per wave packet for the emitter A (resp. B). Hence  $g_{CD}^{(2)}$  can be rewritten as

$$g_{CD}^{(2)}(t, t + \tau) = n_A n_B T^2 e^{-(\gamma_A + \gamma_B)t} e^{-\gamma_B \tau} + n_A n_B R^2 e^{-(\gamma_A + \gamma_B)t} e^{-\gamma_A \tau} - n_A n_B T R e^{-(\gamma_A + \gamma_B)t} e^{-(\gamma_A + \gamma_B^* + \gamma_B^* + \gamma_B^*)\tau/2} \left[ e^{i\Delta\omega\tau} + e^{-i\Delta\omega\tau} \right].$$
(S7)

where  $\Delta \omega = \omega_B - \omega_A$ . Integrating over the two time variables gives

$$\int_{0}^{\infty} dt_{1} \int_{0}^{\infty} d_{2}t_{2} g_{CD}^{(2)}(t_{1}, t_{2}) = 2 \int_{0}^{\infty} dt \int_{0}^{\infty} d\tau g_{CD}^{(2)}(t, t + \tau) 
= \frac{2n_{A}n_{B}}{\gamma_{A} + \gamma_{B}} \int_{0}^{\infty} d\tau \left[ T^{2}e^{-\gamma_{B}\tau} + R^{2}e^{-\gamma_{A}\tau} - TRe^{-(\gamma_{A} + \gamma_{A}^{*} + \gamma_{B} + \gamma_{B}^{*})\tau/2} \left( e^{i\Delta\omega\tau} + e^{-i\Delta\omega\tau} \right) \right] 
= \frac{2n_{A}n_{B}}{\gamma_{A} + \gamma_{B}} \left[ \frac{T^{2}}{\gamma_{B}} + \frac{R^{2}}{\gamma_{A}} - TR \frac{(\gamma_{A} + \gamma_{B} + \gamma_{A}^{*} + \gamma_{B}^{*})}{\Delta\omega^{2} + \left[ (\gamma_{A} + \gamma_{B} + \gamma_{A}^{*} + \gamma_{B}^{*})/2 \right]^{2}} \right].$$
(S8)

On the other hand we have

$$\int_{0}^{\infty} dt \langle \hat{a}_{C}^{\dagger}(t) \hat{a}_{C}(t) \rangle = \int_{0}^{\infty} dt \left[ T \langle \hat{a}_{A}^{\dagger}(t) \hat{a}_{A}(t) \rangle + R \langle \hat{a}_{B}^{\dagger}(t) \hat{a}_{B}(t) \rangle \right] 
= \frac{T n_{A}}{\gamma_{A}} + \frac{R n_{B}}{\gamma_{B}},$$
(S9)

$$\int_{0}^{\infty} dt \langle \hat{a}_{D}^{\dagger}(t) \hat{a}_{D}(t) \rangle = \frac{Rn_{A}}{\gamma_{A}} + \frac{Tn_{B}}{\gamma_{B}}.$$
 (S10)

For a balanced beam splitter (i.e. T = R = 1/2), by plugging Eqs. S8, S9 and S10 in Eq. S1 we obtain

$$p_c = \frac{1}{2}(1 - M_{(A+B)}) \tag{S11}$$

where  $M_{(A+B)}$ , defined as the mean wave packet overlap, is given by

$$M_{(A+B)} = \frac{\gamma_A \gamma_B}{\gamma_A + \gamma_B} \frac{(\gamma_A + \gamma_B + \gamma_A^* + \gamma_B^*)}{\Delta \omega^2 + [(\gamma_A + \gamma_B + \gamma_A^* + \gamma_B^*)/2]^2}.$$
 (S12)

<sup>\*</sup> Electronic address: pascale.senellart@lpn.cnrs.fr

<sup>[</sup>S1] A. Kiraz, M. Atatüre, and A. Imamoğlu, Phys. Rev. A 69, 032305 (2004).